Available online at www.sciencedirect.com
ScienceDirect
Surface Science 600 (2006) 3436–3445
SURFACE SCIENCE
www.elsevier.com/locate/susc

A kinetic model for step flow growth in molecular beam epitaxy

Lev Balykov, Axel Voigt *

Crystal Growth Group, Research Center Caesar, Ludwig-Erhard-Allee 2, 53175 Bonn, Germany

Received 20 December 2005; accepted for publication 23 June 2006
Available online 13 July 2006

Abstract

A terrace–step–kink model for epitaxial step flow growth of steps with no bonds along them is derived from kinetic arguments. The model is combined with an existing model for the steps that have strong bonding along them to describe steps of arbitrary orientation in terms of densities of adatoms, step adatoms and kinks. A planar steady-state solution for a simplified version of the model is constructed and analyzed. Different mass transport mechanisms are modeled that result in different far-from-equilibrium behavior, confirming that edge diffusion is the main factor stabilizing the steps during growth. Furthermore kinetic Wulff shapes are constructed from the calculated step velocities.

Keywords: Epitaxy; Step flow; Kinetic theory

1. Introduction

Thin film growth by molecular beam epitaxy (MBE) is a modern technology of growing single crystals that inherit atomic structures from substrates. It is technologically relevant, experimentally well-explored and a very active area of theoretical research. Modeling of epitaxial growth is a challenging multi-scale problem. Given the fact that the macroscopic evolution of the growing film is directly related to movements of atoms on surfaces and their various bonding configurations, it is appealing to use atomistic scale simulations for a theoretical description of epitaxial growth. However in order to reach the length and time scales of interest for various applications continuum models have to be used. Today a hierarchy of models has been investigated to describe epitaxial growth: From fully atomistic models, via semi-discrete step flow models to continuum models for the height of the growing film. The main challenge in modeling epitaxial growth is to bridge the gap between these different models and to describe growth processes on a continuum scale by incorporating atomistic effects. For a recent review on such attempts we refer to [1,2] and the references therein. Here we will concentrate on how to incorporate a detailed atomistic description of processes in a semi-discrete step flow model. Step flow models can be viewed as a mesoscopic description of crystalline surfaces. On an atomistic scale the surface consists of atomistically flat terraces, which are separated by steps of monoatomic height. As first pointed out by Burton et al. [3] the advancement of these steps, their nucleation and annihilation, can be used to describe the surface morphology. The model is semi-discrete, discrete in the height resolving the atomistic layers, but continuous in the lateral direction, describing the hoping of adatoms on terraces via a diffusion equation. The steps are thus free boundaries for this diffusion equation, evolving according to the adatom fluxes from the terraces.

The basis for our approach to incorporate atomistic details in such a mesoscopic model was given in [4,5]. They introduced a terrace–step–kink model which circumvents the close-to equilibrium assumption in the classical Burton–Cabrera–Frank model [3,6,7], by relating the adatom fluxes from the terraces to the step to kinetic fluxes due to exchange processes between adatoms, step adatoms,

* Corresponding author. Tel.: +49 228 9656 236; fax: +49 228 9656 187.
E-mail addresses: balykov@caesar.de (L. Balykov), voigt@caesar.de (A. Voigt).

0039-6028/$ - see front matter © 2006 Elsevier B.V. All rights reserved.
doi:10.1016/j.susc.2006.06.031

kinks and the crystal itself in an atomistic picture. The model is derived for [1 0 0] steps and assumes right- and left facing kinks to be only of height one. Furthermore only nearest-neighbor interactions are accounted for. Through a more detailed description of the atomistic fluxes we were able to extend the validity of this model to larger kink densities [8,9], which allows us to use it in far-from-equilibrium growth regimes and also for step orientations "$[1\,0\,0]+\theta$", with θ small. However, to simulate epitaxial growth a model is needed, which is valid for all orientations. If we consider island growth, it is clear that a model, which is only valid close to the [1 0 0] direction, is not sufficient. But also in the step flow regime, a step train initially in [1 0 0] direction, will not remain in this direction, due to various instabilities, leading to a meandering of the step and thus local orientations far away from the initial direction.

The [1 0 0] model gives completely wrong results at large deviations from the direction it is derived for. Take equilibrium, for instance: Treating [1 1 0] step as "$[1\,0\,0]+\pi/4$" would give the equilibrium kink density as $k^{\mathrm{eq}}_{[1\,0\,0]+\pi/4} = 2^{-1/2}a^{-1}$, while the correct value should be $k^{\mathrm{eq}}_{[1\,1\,0]} = 2^{-1/2}a^{-1}/2$ (see [3]). Out of equilibrium, the situation is similar, since our "$[1\,0\,0]+\theta$" model does not allow for kinks of heights larger than 1 making most of the processes occurring at [1 0 0] steps impossible at [1 1 0] steps, for example. Here we therefore will extend the previous work to treat also step orientations "$[1\,1\,0]-\theta$", with θ small. We thus propose a compromise solution by having two different models for vicinities of [1 0 0] and [1 1 0] steps.

The outline of the paper is as follows: In Section 2 we review the structure of the terrace–step–kink model introduced in [5] and adapt it to describe [1 1 0] steps. In Section 3 we analyze the model, considering the equilibrium solution and a specially constructed planar steady-state solution and compare the results with the [1 0 0] model. In Section 4 we push the limits of both the [1 0 0] and [1 1 0] model to consider orientations "$[1\,0\,0]+\theta$" and "$[1\,1\,0]-\theta$", such that all orientations are covered and compute kinetic Wulff shapes from specially constructed solutions. Finally we draw conclusions in Section 5.

2. Kinetic step flow model

We denote by Ω the projected domain of a film surface, and assume that Ω is independent of time t. Now, islands or terraces of discrete height i are subsets of this time independent domain and we denote them by $\Omega_i = \Omega_i(t)$, $i = 0, 1, \ldots$ The steps are then the boundaries of these islands or terraces and we denote them by $\Gamma_i = \Gamma_i(t)$, $i = 1, 2, \ldots$ As in the classical Burton–Cabrera–Frank model [3] we denote by $\rho_i = \rho_i(x, y, t)$ the adatom density on terrace $\Omega_i(t)$ at position (x, y) and time t. The adatom diffusion on a terrace is described by the diffusion equation for the adatom density:

$$\partial_t \rho_i - D_T \nabla^2 \rho_i = -\tau^{-1}\rho_i + F_T \quad \text{in } \Omega_i(t), \tag{2.1}$$

where D_T is the adatom diffusion coefficient on a terrace, τ^{-1} is the desorption rate and F_T is the deposition flux rate onto the terrace. Now in contrast to [3] the fluxes of adatoms to the steps are given by

$$-D_T \nabla \rho_i \cdot \vec{n}_i - v_i \rho_i = f_{i,+}, \tag{2.2}$$

$$D_T \nabla \rho_{i-1} \cdot \vec{n}_i + v_i \rho_{i-1} = f_{i,-}, \tag{2.3}$$

where $f_{i,+}$ is the net flux from the upper terrace $\Omega_i(t)$ and $f_{i,-}$ the net flux from the lower terrace $\Omega_{i-1}(t)$ to the boundary $\Gamma_i(t)$, which will be specified. In [3] and various generalizations of it, e.g. [6,7] the definition of these net fluxes assumes the step to be in equilibrium or close to equilibrium. The terrace–step–kink model circumvents this assumption and allows more realistic far-from-equilibrium situations. $\vec{n}_i$ is the unit normal of the step $\Gamma_i(t)$ pointing from the upper to the lower terrace, and v_i is the normal velocity of the step $\Gamma_i(t)$ with the convention that $v_i > 0$ if the movement of $\Gamma_i(t)$ is in the direction of $\vec{n}_i$. The terms $v\rho_i$ describe the convection of adatoms due to the motion of the step and are needed for mass conservation.

In order to define the net fluxes $f_{i,\pm}$ we introduce a step adatom density φ_i and a kink density k_i along each step $\Gamma_i(t)$, $i = 1, 2, \ldots$ The step adatoms diffuse along the moving step $\Gamma_i(t)$ according to

$$\partial_t \varphi_i + v_i(1 + a^2 \varphi_i \kappa_i) - D_E \partial_s^2 \varphi_i = F_{E,i} \tag{2.4}$$

in which D_E is the step adatom diffusion coefficient on a step, $F_{E,i}$ is the net flux rate to the step, v_i the normal velocity of the step, κ_i the mean curvature of the step and ∂_s denoted the derivative with respect to the arc length. The equation holds on a smooth (coarse grained) step. The same is true for the equation for the kink density along the step $\Gamma_i(t)$, which reads

$$\partial_t k_i + \partial_s(w_i(n_{i,r} - n_{i,l})) = 2(g_i - h_i), \tag{2.5}$$

where w_i is the kink velocity on step $\Gamma_i(t)$, g_i the gain due to production of kinks, h_i the loss due to reduction of kinks on step $\Gamma_i(t)$ and $n_{i,r}$ and $n_{i,l}$ denote the density of right and left facing no-kink positions. Among the elementary processes that occur at the step there are those that create or annihilate kinks. Assuming growth (as opposed to etching), we group these processes in g_i and h_i, so that they represent the kink production and reduction rates, respectively. In case of etching, their respective meaning would obviously be reversed. Even if Eqs. (2.4) and (2.5) are defined on a coarse grained smooth step, what we essentially model is the underlying microscopic picture. When we speak of the step adatom diffusion, we essentially mean migration along the straight segment of a close packed step as it is discussed in [10,11], which will come clear in the definition of the quantities F_E, w_i, h_i and g_i. Here we do not automatically consider step adatoms to be a simple pair of kink of opposite sign facing away from each other. When an atom is attached to either side of a step adatom, these sides behave like individual kinks. There are, however, other processes. For instance, a kink is characterized by a velocity, with which it moves along a step. Kinks of opposite sign are expected to move with equal velocities

but in opposite directions. Such a motion of kinks along a step contributes to the step velocity and growth rate. However, when a step adatom moves along a step, both its sides move in the same direction without contributing to growth rate, which means that the two "weak kinks" forming a step adatoms are so strongly bound to each other, that they lose their individual characteristics. Also, in our general treatment we allow for detachment of step adatoms back to the terrace, this process being energetically different from detaching an atom from a kink site. Overall, since two sides of a step adatom do not always act like two kinks, we choose to treat step adatoms as a special species rather than a simple combination of two kinks. Step vacancies, on the other hand, are treated as two kinks facing each other, because both kinks retain their characteristics. In case of etching, the situation might have to be reversed.

Eqs. (2.4) and (2.5) have been introduced in [5] for [1 0 0] steps. However, they are independent of the definition of the fluxes $f_{i,\pm}$ and the terms $F_{E,i}$, w_i, g_i, h_i, and thus can be used for other orientations as well. Until now the model is a general model without any restriction on the crystallographic structure of the film. However by defining the quantities $f_{i,\pm}$, $F_{E,i}$, w_i, g_i and h_i we will restrict ourself to a simple cubic SOS model.

To relate the quantities defined per unit arc length in the macroscopic description to the atomistic description, we need to project them to the [1 1 0] direction. We therefore introduce the projected quantities $\bar{\rho}_i = a^2\rho_i$, $\bar{\varphi}_i = 2^{-1/2}a\varphi_i \cos^{-1}(\theta_i)$, $\bar{k}_{i,r} = 2^{-1/2}ak_{i,r}\cos^{-1}(\theta_i)$, $\bar{k}_{i,l} = 2^{-1/2}ak_{i,l}\cos^{-1}(\theta_i)$, $\bar{n}_{i,r} = 2^{-1/2}an_{i,r}\cos^{-1}(\theta_i)$ and $\bar{n}_{i,l} = 2^{-1/2}an_{i,l}\cos^{-1}(\theta_i)$, which are probabilities per site. Here a is the lattice constant. These projections have been neglected in the previous models for [1 0 0] steps because deviations from this orientation have not been considered. However the models in [8,9] can be modified in the same way if in the definition of the atomistic fluxes the quantities are projected onto [1 0 0] direction.

For [1 0 0] steps, we have the relation $\tan(\theta_i) = \bar{k}_{i,r} - \bar{k}_{i,l}$, with $\bar{k}_{i,r}$ and $\bar{k}_{i,l}$ right and left facing kinks, respectively, and $\bar{k}_i = \bar{k}_{i,r} + \bar{k}_{i,l}$. Here θ_i is the angle between one of the low index crystallographic directions and the normal to the curved step $\Gamma_i(t)$.

For [1 1 0] steps the total density of kinks on $\Gamma_i(t)$ is $\bar{k}_i = \bar{k}_{i,r} = \bar{k}_{i,l}$ and the orientation of the step is given by $\tan(\theta_i) = 0.5(\bar{n}_{i,r} - \bar{n}_{i,l})$. Here θ_i is between [1 1 0] direction and the step. We further have the constraint $\bar{n}_{i,r} = 1 + \tan\theta - \bar{k}_{i,r}$ and $\bar{n}_{i,l} = 1 - \tan\theta - \bar{k}_{i,l}$, which results from $\bar{n}_{i,r} + \bar{n}_{i,l} + \bar{k}_{i,r} + \bar{k}_{i,l} = 2$.

A definition of the fluxes $f_{i,\pm}$ for [1 0 0] steps is given in [8,9]. Here we derive the corresponding fluxes for [1 1 0] steps. We thus now define the quantities $F_{E,i}$, w_i, g_i and h_i for [1 1 0] steps and relate them to the fluxes $f_{i,\pm}$ in Eqs. (2.2) and (2.3). By doing so we go to an atomistic description of the step and consider all possible ways how an adatom and a step adatom can be incorporated into the crystal lattice. Within a mean field assumption all possible processes which include adatoms on the upper (+) or lower (−) terrace are illustrated in Fig. 1.

To define the fluxes let us consider an example: an adatom from $\Omega_{i-1}(t)$ becomes a step adatom on $\Gamma_i(t)$ on a straight right-facing segment (f_{12}^-) (see Fig. 2). The probability to have an adatom is $\bar{\rho}_{i-1}$. We need to have two no kink positions to be able to generate a new step adatom. The probability is $\bar{n}_{i,r}^2$. Furthermore we do not want the position to be already occupied by a step adatom. The probability to find an open position is $(1 - \bar{\varphi}_i)$. The hopping rate is given by $D_{TE}^- a^{-2}$, where "−" indicates the hopping from the lower terrace "T" to the step "E". The contribution to the flux f_{12}^- due to attachment is thus given by $\bar{\rho}_{i-1}\bar{n}_{i,r}^2(1 - \bar{\varphi}_i)D_{TE}^- a^{-2}$. We also need to take the opposite process into account to incorporate desorption from the step $\Gamma_i(t)$ back to the terrace $\Omega_{i-1}(t)$. The probability to have one step adatom on a right facing straight segment is $\bar{\varphi}_i$, in addition we again need two no kink positions $\bar{n}_{i,r}^2$ and an open position on the terrace to hop on $(1 - \bar{\rho}_{i-1})$. We multiply by the hopping rate $D_{ET}^- a^{-2}$. This gives the contribution to f_{12}^- due to detachment $-\bar{\varphi}_i\bar{n}_{i,r}^2(1 - \bar{\rho}_{i-1})D_{ET}^- a^{-2}$. Adding both gives the definition of f_{12}^-. All other fluxes can be computed in the same way and lead to the following definitions corresponding to the processes illustrated in Fig. 1. The notation is chosen in such that in $f_{kl}^{\pm}$, + and − indicate the upper and lower terrace, respectively, $k = 1, 2$ indicate processes which do not change or change the density of kinks,

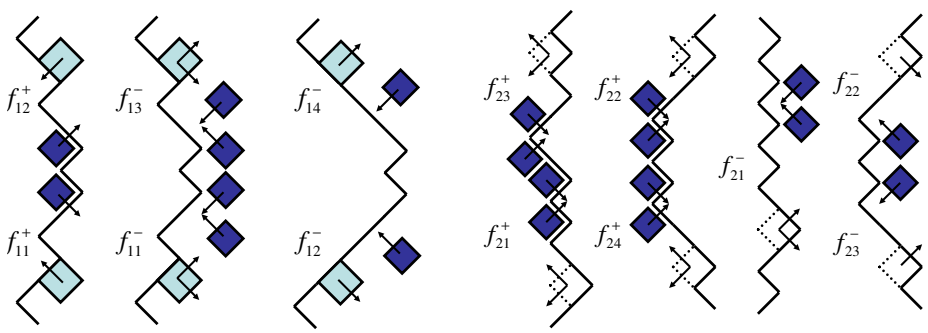

Fig. 1. Microscopic fluxes between the upper and lower terrace and a step, that explicitly change the density of adatoms, step adatoms (left) and kinks (right). Adatoms (dark gray), step adatoms (light gray), kinks (white), dotted contours depict atoms inside the bulk.

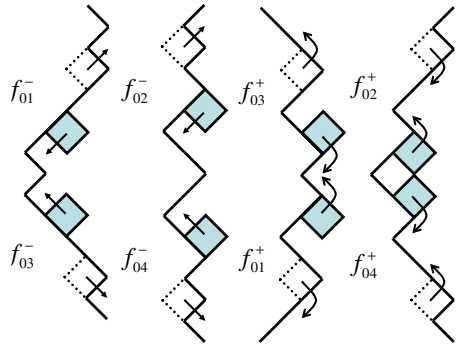

Fig. 2. Microscopic fluxes between a step and a kink site, that explicitly change the density of step adatoms and kinks. Step adatoms (light gray), kinks (white), dotted contours depict atoms inside the bulk.

respectively, and $l = 1, 2, \ldots$ is a numbering of the different possibilities:

$$f_{11}^+ = D_{TE}^+ a^{-2} \bar{n}_{i,r}(1-\bar{\varphi}_i)\bar{\rho}_i - D_{ET}^+ a^{-2}\bar{n}_{i,r}(1-\bar{\rho}_i)\bar{\varphi}_i, \quad (2.6)$$

$$f_{12}^+ = D_{TE}^+ a^{-2} \bar{n}_{i,l}(1-\bar{\varphi}_i)\bar{\rho}_i - D_{ET}^+ a^{-2}\bar{n}_{i,l}(1-\bar{\rho}_i)\bar{\varphi}_i, \quad (2.7)$$

$$f_{21}^+ = 2D_{TK}^+ a^{-2}\bar{\rho}_i\bar{k}_i^3 - 2D_{KT}^+ a^{-2}(1-\bar{\rho}_i)\bar{k}_i\bar{n}_{i,r}\bar{n}_{i,l}, \quad (2.8)$$

$$f_{22}^+ = 2D_{TK}^+ a^{-2}\bar{\rho}_i\bar{k}_i^2\bar{n}_{i,r} - 2D_{KT}^+ a^{-2}(1-\bar{\rho}_i)\bar{k}_i^2\bar{n}_{i,r}, \quad (2.9)$$

$$f_{23}^+ = 2D_{TK}^+ a^{-2}\bar{\rho}_i\bar{k}_i\bar{n}_{i,r}\bar{n}_{i,l} - 2D_{KT}^+ a^{-2}(1-\bar{\rho}_i)\bar{k}_i^3, \quad (2.10)$$

$$f_{24}^+ = 2D_{TK}^+ a^{-2}\bar{\rho}_i\bar{k}_i^2\bar{n}_{i,l} - 2D_{KT}^+ a^{-2}(1-\bar{\rho}_i)\bar{k}_i^2\bar{n}_{i,l}, \quad (2.11)$$

which include all processes in which adatoms on the upper terrace are involved, and

$$f_{11}^- = 2D_{TE}^- a^{-2}\bar{n}_{i,r}\bar{k}_i(1-\bar{\varphi}_i)\bar{\rho}_{i-1} - 2D_{ET}^- a^{-2}(1-\bar{\rho}_{i-1})\bar{n}_{i,r}\bar{k}_i\bar{\varphi}_i, \quad (2.12)$$

$$f_{12}^- = D_{TE}^- a^{-2}\bar{n}_{i,r}^2(1-\bar{\varphi}_i)\bar{\rho}_{i-1} - D_{ET}^- a^{-2}(1-\bar{\rho}_{i-1})\bar{n}_{i,r}^2\bar{\varphi}_i, \quad (2.13)$$

$$f_{13}^- = 2D_{TE}^- a^{-2}\bar{n}_{i,l}\bar{k}_i(1-\bar{\varphi}_i)\bar{\rho}_{i-1} - 2D_{ET}^- a^{-2}(1-\bar{\rho}_{i-1})\bar{n}_{i,l}\bar{k}_i\bar{\varphi}_i, \quad (2.14)$$

$$f_{14}^- = D_{TE}^- a^{-2}\bar{n}_{i,l}^2(1-\bar{\varphi}_i)\bar{\rho}_{i-1} - D_{ET}^- a^{-2}(1-\bar{\rho}_{i-1})\bar{n}_{i,l}^2\bar{\varphi}_i, \quad (2.15)$$

$$f_{21}^- = 2D_{TK}^- a^{-2}\bar{\rho}_{i-1}\bar{k}_i^3 - 2D_{KT}^- a^{-2}\bar{k}_i(1-\bar{\rho}_{i-1})\bar{n}_{i,r}\bar{n}_{i,l}, \quad (2.16)$$

$$f_{22}^- = D_{TK}^- a^{-2}\bar{\rho}_{i-1}\bar{k}_i^2\bar{n}_{i,r} - 2D_{KT}^-(1-\bar{\rho}_{i-1})\bar{k}_i^2\bar{n}_{i,r}, \quad (2.17)$$

$$f_{23}^- = D_{TK}^- a^{-2}\bar{\rho}_{i-1}\bar{k}_i^2\bar{n}_{i,l} - 2D_{KT}^-(1-\bar{\rho}_{i-1})\bar{k}_i^2\bar{n}_{i,l} \quad (2.18)$$

for processes in which adatoms on the lower terrace are involved (see Fig. 1). All fluxes are defined per unit site projected onto [1 1 0] direction. The diffusion coefficients D_{XY}^+ indicate hopping from X to Y, with $X, Y = T$ (terrace), E (edge), K (kink). The differences in D_{TE}^+ and D_{TE}^-, D_{TK}^+ and D_{TK}^-, as well as in their inverse counterparts model the Ehrlich–Schwoebel effect [12,13]. In order to relate these fluxes, which are defined per unit site in [1 1 0] direction to $f_{i,+}$ in Eq. (2.2) and $f_{i,-}$ in Eq. (2.3), defined per unit area on the curved step, we need to multiply by $2^{1/2}a^{-1}\cos(\theta_i)$. Thus

$$f_{i,+} = (f_{11}^+ + f_{12}^+ + f_{21}^+ + f_{22}^+ + f_{23}^+ + f_{24}^+)2^{1/2}a^{-1}\cos\theta_i, \quad (2.19)$$

$$f_{i,-} = (f_{11}^- + f_{12}^- + f_{12}^- + f_{14}^- + f_{21}^- + f_{22}^- + f_{23}^-)2^{1/2}a^{-1}\cos\theta_i. \quad (2.20)$$

In order to define $F_{E,i}$ in Eq. (2.4), we have in addition to the contribution from the upper and lower terraces f_1^+ and f_1^-, respectively, with $f_1^+ = f_{11}^+ + f_{12}^+$ and $f_1^- = f_{11}^- + f_{12}^- + f_{13}^- + f_{14}^-$, to consider exchange processes between step adatoms and kinks. The corresponding fluxes are

$$f_{01}^+ = D_{EK}^+ a^{-2}\bar{\varphi}_i\bar{k}_i^3\bar{n}_{i,r} - D_{KE}^+ a^{-2}(1-\bar{\varphi}_i)\bar{k}_i\bar{n}_{i,r}^2\bar{n}_{i,l}, \quad (2.21)$$

$$f_{02}^+ = D_{EK}^+ a^{-2}\bar{\varphi}_i\bar{k}_i^2\bar{n}_{i,r}^2 - D_{KE}^+ a^{-2}(1-\bar{\varphi}_i)\bar{k}_i^2\bar{n}_{i,r}^2, \quad (2.22)$$

$$f_{03}^+ = D_{EK}^+ a^{-2}2\bar{\varphi}_i\bar{k}_i^3\bar{n}_{i,l} - D_{KE}^+ a^{-2}(1-\bar{\varphi}_i)\bar{k}_i\bar{n}_{i,r}\bar{n}_{i,l}^2, \quad (2.23)$$

$$f_{04}^+ = D_{EK}^+ a^{-2}\bar{\varphi}_i\bar{k}_i^2\bar{n}_{i,l}^2 - D_{KE}^+ a^{-2}(1-\bar{\varphi}_i)\bar{k}_i^2\bar{n}_{i,l}^2 \quad (2.24)$$

for processes from above and

$$f_{01}^- = D_{EK}^- a^{-2}\bar{\varphi}_i\bar{k}_i^2\bar{n}_{i,r} - D_{KE}^- a^{-2}(1-\bar{\varphi}_i)\bar{k}_i^2\bar{n}_{i,r}, \quad (2.25)$$

$$f_{02}^- = D_{EK}^- a^{-2}\bar{\varphi}_i\bar{k}_i\bar{n}_{i,r}\bar{n}_{i,l} - D_{KE}^- a^{-2}(1-\bar{\varphi}_i)\bar{k}_i^3, \quad (2.26)$$

$$f_{03}^- = D_{EK}^- a^{-2}\bar{\varphi}_i\bar{k}_i^2\bar{n}_{i,l} - D_{KE}^- a^{-2}(1-\bar{\varphi}_i)\bar{k}_i^2\bar{n}_{i,l}, \quad (2.27)$$

$$f_{04}^- = D_{EK}^- a^{-2}\bar{\varphi}_i\bar{k}_i\bar{n}_{i,r}\bar{n}_{i,l} - D_{KE}^- a^{-2}(1-\bar{\varphi}_i)\bar{k}_i^3 \quad (2.28)$$

for processes from below (see Fig. 2). The differences in D_{EK}^+ and D_{EK}^- as well as D_{KE}^+ and D_{KE}^- model the kink Ehrlich–Schwoebel effect, e.g. [14–16]. For simplicity we assume the same diffusion coefficients for left- and right-facing kinks. Again we need to relate these fluxes defined per unit site in [1 1 0] direction to $F_{E,i}$ through $2^{1/2}a^{-1}\cos(\theta_i)$

$$F_{E,i} = (f_{11}^+ + f_{12}^+ + f_{11}^- + f_{12}^- + f_{13}^- + f_{14}^-)2^{1/2}a^{-1}\cos\theta_i.$$

Due to the attachment of adatoms and step adatoms into kinks, the kinks move along the step. The velocities for left- and right-facing kinks are $-w_i$ and w_i, respectively. The resulting convective flux of kinks with respect to s is $w_i(n_{i,r} - n_{i,l}) = w_i 2^{3/2}a^{-1}\sin\theta_i$ with

$$w_i = \frac{a}{\bar{n}_{i,r} + \bar{n}_{i,l}}(f_{22}^+ + f_{24}^+ + f_{22}^- + f_{23}^- + f_{02}^+ + f_{04}^+ + f_{01}^- + f_{03}^-)2^{1/2}\cos\theta_i.$$

The gain due to kink production is

$$g_i = (f_{23}^+ + f_{02}^- + f_{04}^-)2^{1/2}a^{-1}\cos\theta_i$$

and the loss due to kink reduction is

$$h_i = (f_{21}^+ + f_{21}^- + f_{01}^+ + f_{03}^+)2^{1/2}a^{-1}\cos\theta_i.$$

For the velocity law, describing the movement of the steps $\Gamma_i(t)$ in normal direction, we take the same form as for the [1 0 0] model with k_i being replaced by $\bar{n}_{i,r} + \bar{n}_{i,l}$

$$v_i = w_i(\bar{n}_{i,r} + \bar{n}_{i,l}) + (g_i + h_i)a^2. \quad (2.29)$$

3. Equilibrium and planar steady-state solution

3.1. Equilibrium and detailed balance

As in the [1 0 0] model [8,9] we first consider equilibrium. At equilibrium, $\rho_i = \rho$. The principle of detailed balance

requires that all fluxes $f_{kl}^{\pm} = 0$. From these assumptions it follows for equilibrium density of adatoms, edge adatoms and kinks

$$\bar{\rho}_i^{\mathrm{eq}} = \frac{D_{KT}^{\pm}}{D_{KT}^{\pm} + D_{TK}^{\pm}}, \tag{3.30}$$

$$\bar{\varphi}_i^{\mathrm{eq}} = \frac{D_{KE}^{\pm}}{D_{KE}^{\pm} + D_{EK}^{\pm}}, \tag{3.31}$$

$$\bar{k}_i^{\mathrm{eq}} = \frac{1}{2}, \tag{3.32}$$

which is the same as for the [1 0 0] model for $\bar{\rho}_i^{\mathrm{eq}}$ and $\bar{\varphi}_i^{\mathrm{eq}}$. The equilibrium kink density coincides with BCF's expression for the kink density for the corresponding case. With expressions (3.30)–(3.32) for adatoms, step adatoms and kinks, all expressions for $f_{kl}^{\pm} = 0$ are satisfied identically and provide consistency conditions, which restrict the possible values of the diffusion coefficients. The remaining coefficients D_T, D_E and $D_{XY}^{\pm}$ with $X, Y = T, E, K, B$ are defined through $D = l^2 \nu$, with l^2 the mean square distance covered by a single jump and $\nu = \nu_0 \exp\left(-\frac{E}{k_{\mathrm{B}}T}\right)$, the jump rate, with ν_0 the attempt frequency and $E = E_{\mathrm{t}} - E_{\mathrm{b}}$ the energy barrier that has to be overcome, with E_{t} the transition state energy and E_{b} the binding energy. As in the [1 0 0] model these are the only remaining parameters in the model, they can in principle be computed ab initio, which turns the equations into a parameter free model.

3.2. Planar steady-state solution

We now consider as in the [1 0 0] model the simplest conceivable statistical mechanics model of a crystal surface, a cubic solid-on-solid (SOS) model and analyze a planar steady-state solution for a periodic sequence of steps, separated by distance $2L$ and moving at velocity $v = v_i$, $i = 1, 2, \ldots$ along the [1 1 0] direction. From the constructed equations, which are identical to the ones derived for the [1 0 0] model, we can calculate steady-state values for the densities of kinks, step adatoms and adatoms on terraces near the step. We define the dimensionless edge Peclet number $P_{\mathrm{step}} = 2a^3 F_T L / D_E$ and the calculations are done with $D_E = 10^7$ and $L = 10^4$.

3.2.1. Kink density

Equilibrium kink density does not depend on either the terrace or edge diffusion coefficients and is equal to $\bar{k}_i^{\mathrm{eq}} = 1/2$. Out of equilibrium, kink density starts to change (see Fig. 3). We can see that at very small edge Peclet numbers the kink density is almost constant, then it starts decreasing, i.e., the step roughens, and with further increase of the edge Peclet number asymptotically approaches a certain constant. This means that [1 1 0] steps do not fall apart into large segments of [1 0 0] steps but are rather stable even far-from equilibrium. It turns out that this asymptotic value is almost independent of either the terrace or edge diffusion coefficients, while the value

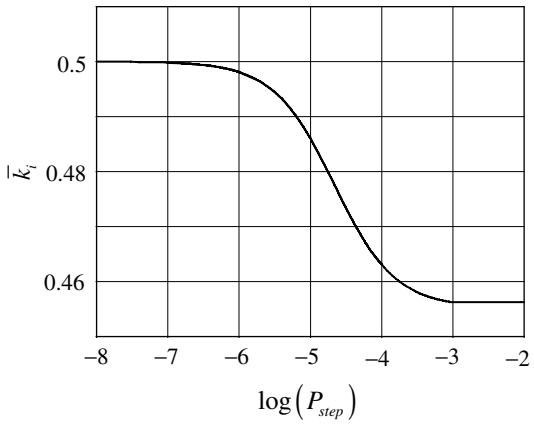

Fig. 3. Kink density as a function of the edge Peclet number.

of the edge Peclet number, at which the kink density starts switching from its equilibrium value to the far-from-equilibrium value, depends on those coefficients. Unlike kink density along [1 0 0] step, we do not observe any scaling law for the kinks as a function of the edge Peclet number. The stabilization, keeping the step in the [1 1 0] direction results from edge diffusion, which will be shown by comparing the step roughness if edge diffusion is allowed and suppressed.

3.2.2. Step adatom and adatom density

Step adatoms and adatoms on terraces behave very similarly. Their densities are almost constant at very small edge Peclet numbers, then gradually increase and approach linear dependence on the edge Peclet number far-from equilibrium (see Figs. 4 and 5). Therefore, far-from-equilibrium adatom and edge adatom densities scale linearly with the edge Peclet number. This is consistent with the kink density being constant. If the kink density does not change with increase of Peclet number, i.e., by increasing deposition flux, all the extra material must go into adatoms and step adatoms. Linear scaling for both adatoms and step adatoms means that far-from equilibrium the step adatom density is linear with respect to adatom density, which is

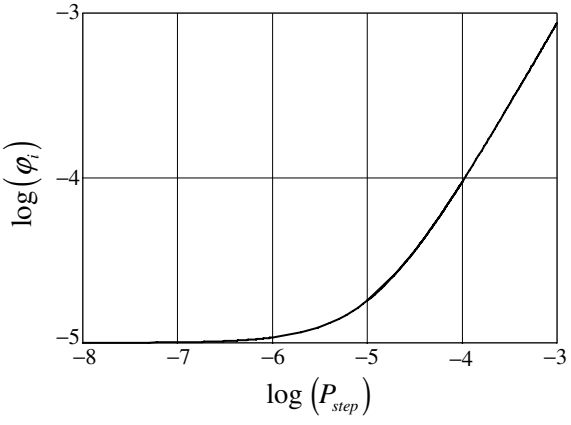

Fig. 4. Step adatom density as a function of the edge Peclet number.

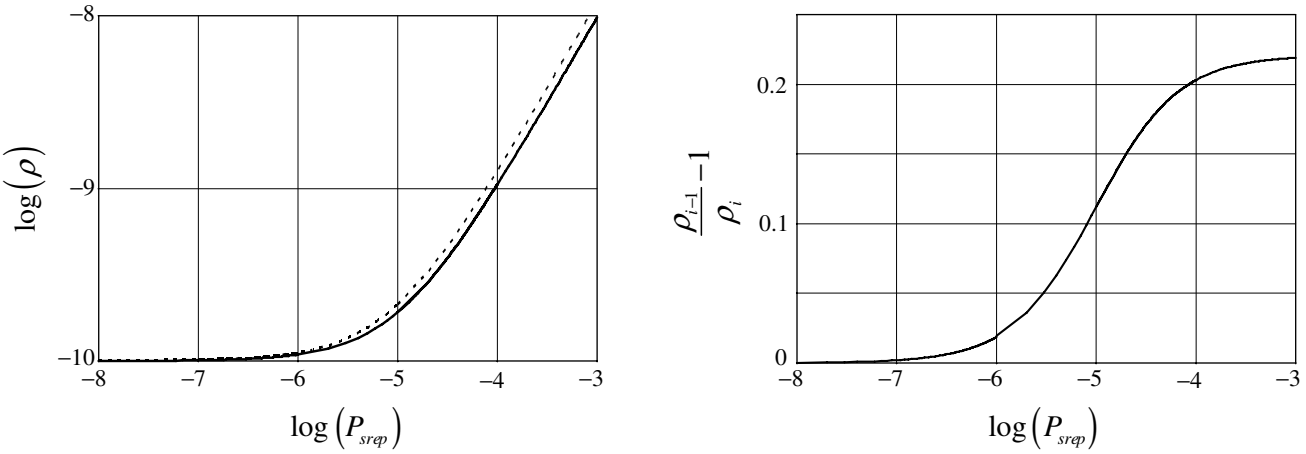

Fig. 5. Adatom density as a function of the edge Peclet number. Solid line corresponds to the density on the upper terrace, dashed to the density on the lower terrace (left). Relative difference of the adatom densities on the upper and lower terrace (right).

expected, since we have no non-linear processes involving adatom–step adatom interactions, such as one-dimensional nucleation. The non-linear correction factors $(1-\bar{\varphi})$ and $(1-\bar{\rho})$ are both very close to unity and do not influence the observed linear dependency.

The upper and lower terrace adatom densities show an asymmetry. As for the [1 0 0] step, this results in an effective inverse Ehrlich–Schwoebel barrier. At very small Peclet numbers the adatom densities on the terraces are almost symmetric, while far-from equilibrium the lower terrace is about 20% more densely populated near the step than the upper terrace (see Fig. 5). Thus as in the [1 0 0] model, depending on the step configuration the asymmetry might lead to step bunching, whereas an energetic difference in the attachment and detachment processes from the upper and lower terrace, due to the Ehrlich–Schwoebel barrier might lead to step meandering. So both instabilities could appear simultaneously on a surface, as experimentally observed in [17] or obtained by KMC simulations [18]. On the other side, depending on the local step configuration, both effects, the effective inverse Ehrlich–Schwoebel effect and the usual step Ehrlich–Schwoebel barrier can also eliminate each other. Computations demonstrating this for [1 0 0] steps are shown in [19].

3.2.3. Mass transport mechanisms

Since we have included many different processes into our model, we can simulate various mass transport mechanisms by blocking some of the processes. In case of [1 0 0] step it resulted in different scaling exponents for different mass transport mechanisms. We consider several different scenarios for the [1 1 0] step. Of course, there are many more options but these are the most illustrative. The results are shown in Fig. 6.

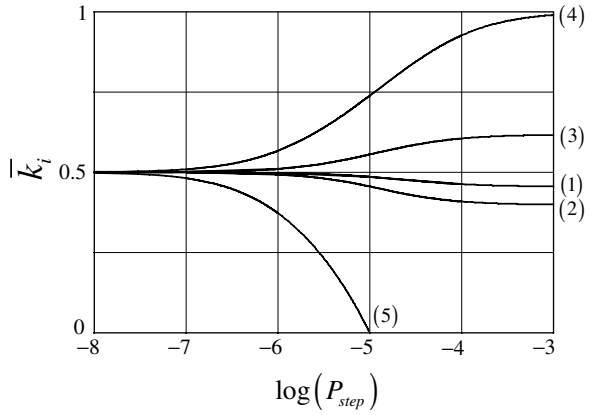

Fig. 6. Kink density as a function of the edge Peclet number for the different mass transport mechanisms (1)–(5).

1. *General case.* This is the case we have described so far. All processes are possible. The step starts to roughen with increase of the edge Peclet number but then the kink density saturates and does not decrease below approximately 0.45. We obtain an effective inverse Ehrlich–Schwoebel barrier from the asymmetry in the adatom concentration.
2. *No edge diffusion.* The step roughens until the kink density reaches 0.40, so the roughening is a little stronger than in the general case, which indicates that edge diffusion has a stabilizing effect on the step. Again we observe an effective inverse Ehrlich–Schwoebel barrier.
3. *No direct adsorption.* Processes of direct interaction between terraces and bulk sites are blocked, thus adatoms first become edge adatoms, which are then incorporated into kinks. Thus edge diffusion is the only mass transport mechanism. The steps start to smoothen but stops at 0.61. Here we observe an effective normal Ehrlich–Schwoebel barrier.
4. *No direct adsorption and infinitely large normal kink Ehrlich–Schwoebel barrier.* In this case step adatoms cannot jump into kinks from above. This results in the extreme case of step smoothening [20] when the kink

density approaches unity and indicates that it is the sliding of step adatoms into kinks from below that has a stabilizing effect on the step structure [14], while jumping of step adatoms into kinks from above resist that stabilization.

5. *No direct adsorption and infinitely large inverse kink Ehrlich–Schwoebel barrier.* In this case step adatoms cannot slide into kinks from below. The [1 1 0] step separates itself into very long kink-free segments and we can no longer apply our model as these segments have to be treated as [1 0 0] steps, for example, we will have to include negative kinks. This case is most likely to be unphysical. We only use it to further illustrate the point that while attachment of step adatoms by sliding into kink from below stabilizes the structure, attachment by jumping down into kink from above has the opposite effect.

The first three cases correspond to the special cases we considered in our [1 0 0] model (see [9]). The main results are very similar: edge diffusion stabilizes the step as it is rougher during growth without edge diffusion. The difference is that the effect of edge diffusion on the [1 1 0] step is so strong that the step can actually become smoother than in equilibrium. But this has already been reported [20]. The last two cases are variations of the third case and have not been analyzed for the [1 0 0] model.

4. Dependency on the angle θ

Until now we have analyzed the models for [1 0 0] steps (see [8,9]) and [1 1 0] steps only in the crystallographic orientations they are derived for. However these models are also valid for orientations "$[100]+\theta$" and "$[110]-\theta$", for small values of θ, respectively. We will consider here results from the equilibrium and planar steady-state solutions of both models for different values of θ.

4.1. Equilibrium properties

Fig. 7 shows the equilibrium kink density for both models as a function of θ. We compare the equilibrium kink density with the expression derived in [3], which we correct to include the change of unit length. We obtain a good agreement for small angles with the [1 0 0] model and for large angles with the [1 1 0] model.

Another equilibrium property of interest is the step stiffness or the step free energy. Within a similar model for [1 0 0] steps Margetis and Caflisch [21] compute the step stiffness as a function of orientation close to the [1 0 0] direction. The obtained functional form is close to the recent derivations of Stasevich et al. [22]. We do not intend to compute the angular dependence of the step stiffness here, but rather are interested in kinetic properties as they are assumed to play an even more important role in epitaxial growth, as a far-from-equilibrium growth process [23].

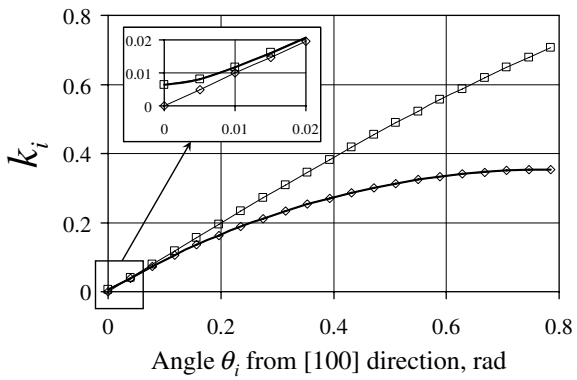

Fig. 7. Equilibrium kink density in the "$[100]+\theta$" and "$[110]-\theta$" model. The equilibrium kink density is computed for each value of θ and shown as a function of θ. □ denotes the [1 0 0] model, ◊ denotes the [1 1 0] model and — denotes the BCF model, which is corrected to account for changes in unit length.

4.2. Kinetic properties

Out of equilibrium, the two models lead to quantitatively different results, thus we do not intend to extend either of the models to large angles. However, we do not expect any special effects occurring at steps of such direction either. Any direction away from a low index crystallographic orientation has additional geometric kinks, which will contribute to the growth process. Thus these directions are assumed to grow faster than the low index crystallographic directions, and thus will not be present during growth.

We now consider the normal velocity for various orientations. The normal velocity of a step in the planar steady-state setting is independent of the direction of a step and, therefore, of its structure, and be always equal to $2FL$, where F is the deposition flux and $2L$ is the distance between the steps. What we do in our model essentially is classify atoms on the surface into three types that are distinguished by the number of lateral bonds they have – adatoms on terraces with no lateral bonds, step adatoms with one lateral bond and step (or bulk) atoms with two or more lateral bonds. Then it is clear that the growth rate should include all the processes that convert terrace and edge adatoms into bulk atoms, minus the opposite processes. This is simply the mass conservation requirement. Therefore, when the densities of adatoms, step adatoms and kinks do not change in time, all of the deposition flux must contribute to the step velocity. We define step velocity in terms of various microscopic fluxes that contribute either to kink velocity, kink creation or kink annihilation. None of these fluxes explicitly contain either F or $2L$, they only enter the model through the boundary conditions for adatom density and the step. Thus, calculating step velocity and comparing it with $2FL$ is a good check of the model's consistency. We did the consistency check for planar

steady-state solution in both models for various angles and it confirmed that both our models are mass-conserving. Another point is the definition of the step velocity itself. Based on the mass conservation arguments, we have derived a velocity law that contains terms accounting for the motion of kinks along a step as well as for creation and annihilation of kink pairs. This velocity law is a very general expression that is valid for steps of any direction. Conventionally, it is assumed that growth only occurs at kink sites [6]. Our expression for the step velocity, Eq. (2.29) allows us to determine quantitatively the contribution of the kink creation g and annihilation h processes to growth. We calculate the ratio of the fluxes corresponding to creation and annihilation of kinks and the fluxes corresponding to the kink motion. We see that in the vicinity of [1 0 0] step the contribution from the creation and annihilation of kinks is small and the conventional expression $v_i = a w_i k_i \cos(\theta_i)$, used in [6,5], is a fairly good approximation for the step velocity. In the vicinity of [1 1 0] step the contribution from the creation and annihilation of kinks is very essential and cannot be neglected (see Fig. 8). However for a step of any direction, mass is not exactly conserved without taking these processes into account.

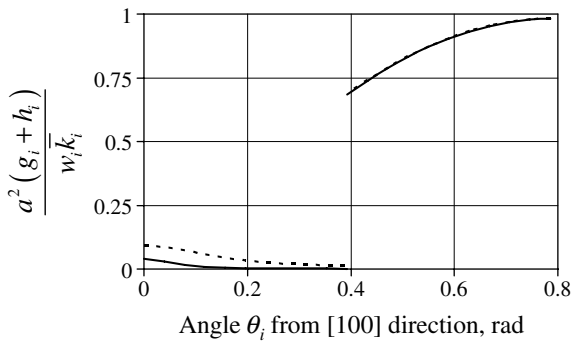

Fig. 8. Importance of kink creation–annihilation terms compared to kink velocity in estimating step velocity. Solid lines correspond to $F = 0.1$, dashed lines to $F = 1.0$.

4.3. Kinetic Wulff shape

In a crystal at equilibrium, the distances of the faces from the center of the crystal are proportional to their surface free energies per unit area, which determines the Wulff shape [24]. However, crystals that grow under the control of interfacial kinetic processes tend asymptotically toward a "kinetic Wulff shape," the analogue of the Wulff shape, except it is based on the anisotropic interfacial kinetic coefficient (see e.g. [25]).

The kinetic Wulff shape can not be computed from the planar steady state of an equidistant sequence of steps. But both our models, for [1 0 0] and [1 1 0] steps can be modified to treat single steps instead of trains of steps. This can be done as follows: instead of using the deposition flux as an external parameter and solving adatom diffusion equation on the terrace with boundary conditions at the steps, we introduce the supersaturation of adatoms near the step. In this case, steps do not feel each other and their structure will not depend on the step-to-step distance. In this limit we have a different type of boundary condition in our system that does not require global mass conservation. So instead of (2.2) and (2.3) we consider in the definition of $f_{i,+}$, $f_{i,-}$, $F_{E,i}$, w_i, g_i and h_i

$$\rho_i = \rho^{\mathrm{eq}}(1 + \sigma_i), \tag{4.33}$$

$$\rho_{i-1} = \rho^{\mathrm{eq}}(1 + \sigma_{i-1}), \tag{4.34}$$

with $\sigma_{i,i-1}$ the supersaturation near the step. In this case the adatom density is independent of the step orientation and we can expect that the step velocity will become angle-dependent, which will allow us to numerically construct a kinetic Wulff shape.

First we use our [1 0 0] model with angles up to $\pi/4$ to calculate the velocities of steps at the steady state and plot

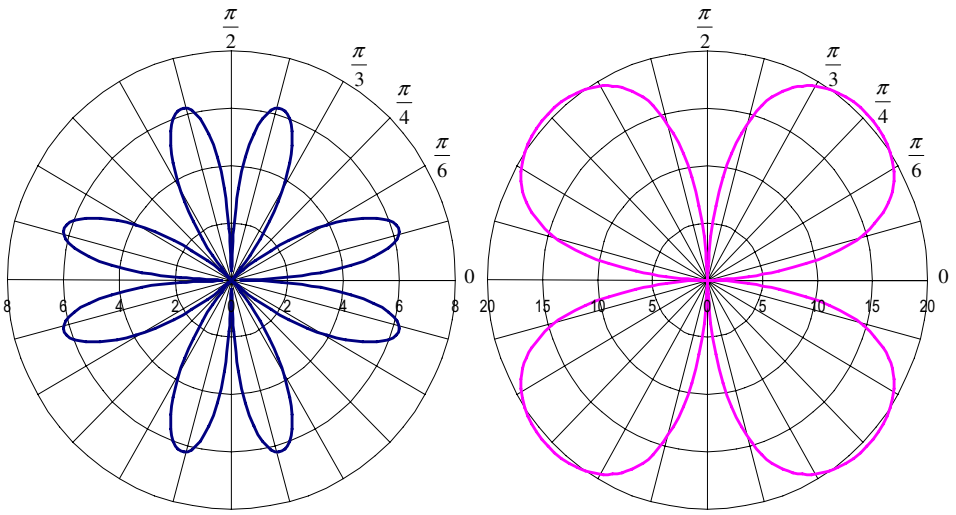

Fig. 9. Angular dependency of velocity obtained from [1 0 0] model (right) and [1 1 0] model (left). Radial scale is in units length per unit time.

these velocities in polar coordinates. The angular velocity diagram is shown in Fig. 9 (right). It shows how fast steps of different orientations would grow. It has cusps at around 0, π/2, π and 3π/2 suggesting that [1 0 0]-like steps will grow slower than their vicinal steps, so [1 0 0] facets may develop during growth if we start from a circular island. Another thing that we see is that [1 1 0]-like steps grow even slower the [1 0 0]-like steps. In fact, they are completely blocked from growing at all, which means that if we start growing a circular island, it will gradually become a perfect diamond and will just stop growing, which is of course wrong and only shows the limits of the [1 0 0] model. With increasing deviation from [1 0 0] direction, the importance of kinks of multiple height increases, while the [1 0 0] model only considers single kinks. Obviously, it underestimates the step velocity at larger angles.

Now let us do the same for our [1 1 0] model. Again we use the model for angles of up to π/4 and plot the velocity in polar coordinates (see Fig. 9 (left)). The [1 1 0] step grows faster than any other step and the [1 0 0] steps are blocked from growing. The reason is the same as before, at π/4 the kink density is zero and no processes are possible within the [1 1 0] model. Thus, the [1 1 0] model fails at large angles. Since it neglects negative kinks and one-dimensional nucleation, it also underestimates the step velocity. Thus, until we have a model that is accurate for any direction, which is not

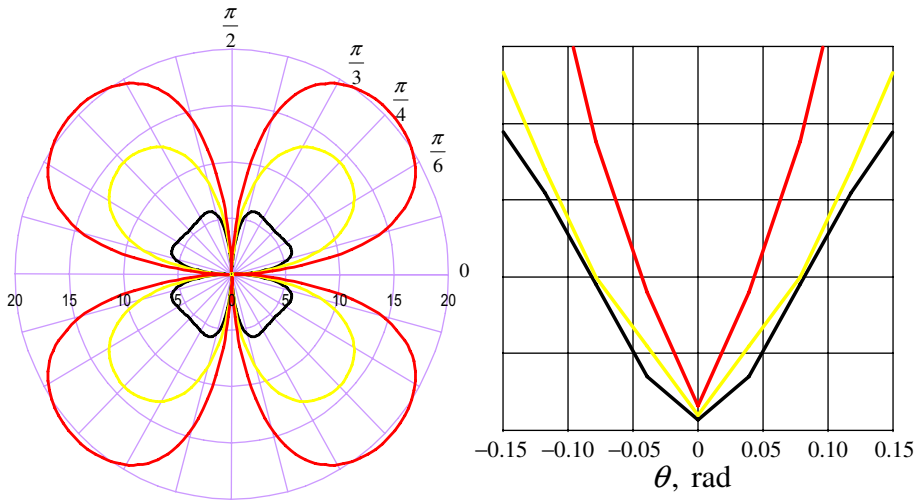

Fig. 10. Angular dependency of velocity obtained from a combination of [1 0 0] and [1 1 0] model for different mass transport mechanisms (left). Enlargement of the cusps near 0 in a Cartesian coordinate system (right). The lines correspond to cases 1–3 in Section 3.2.3: (red) general case, (yellow) no edge diffusion and (black) no direct adsorption. Radial scale is in units length per unit time. (For interpretation of the references in colour in this figure legend, the reader is referred to the web version of this article.)

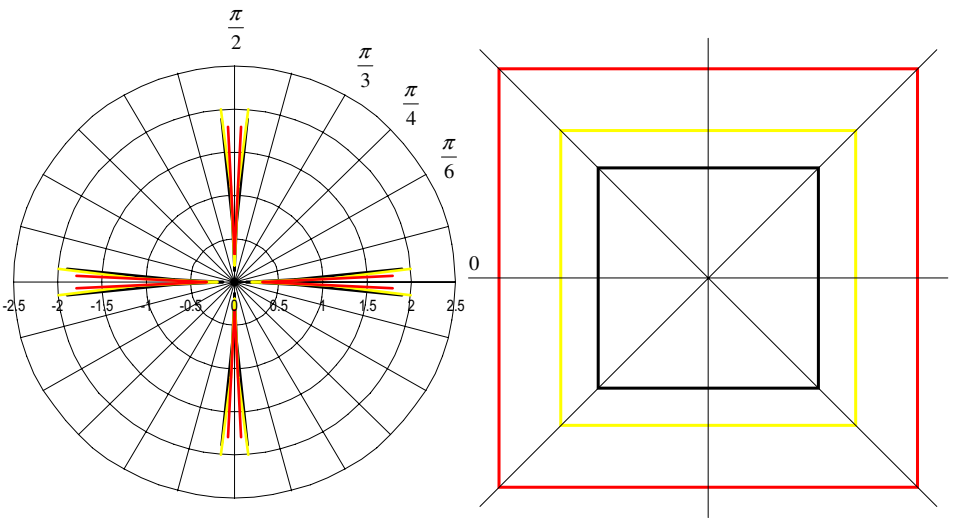

Fig. 11. Kinetic Wulff shape obtained from the combination of the [1 0 0] and [1 1 0] model. Enlargement of Fig. 10 with corresponding Wulff shapes (left) and enlarged Wulff shapes (right). The lines correspond again to cases 1–3 in Section 3.2.3: (red) general case, (yellow) no edge diffusion and (black) no direct adsorption. Radial scale is in units length per unit time. (For interpretation of the references in colour in this figure legend, the reader is referred to the web version of this article.)

yet derived, we can roughly estimate the angular dependence of the step velocity by taking the larger value of the step velocity given by [1 0 0] and [1 1 0] models. This estimation contains an implicit assumption that nothing special happens at directions other than [1 0 0] and [1 1 0]. The resulting plot is shown in Fig. 10. The plot has cusps at 0, $\pi/2$, π and $3\pi/2$ suggesting that the shape of a growing island would be a square bounded by [1 0 0]-like facets.

We now plot the kinetic Wulff shape for the three different mass transport mechanisms described in Section 3.2.3, resulting from the angular dependency of the velocity (see Fig. 11). The plot shows the suggested square as the kinetic Wulff shape with [1 0 0]-like facets for all three mass transport mechanisms.

5. Conclusions

In contrast to the boundary conditions in the Burton–Cabrera–Frank model, which assume a close-to-equilibrium situation, we construct a kinetic model, which is also valid far-from-equilibrium. The only remaining parameters in this model are kinetic hopping rates for a given set of microscopic processes. These are essentially the same parameters as used in kinetic Monte Carlo (KMC) models, and can be computed from first principles. Thus the constructed model combines a detailed microscopic description with the computational efficiency of numerical methods for differential equations.

Within a simple cubic solid-on-solid model, we consider two different step orientations, [1 0 0] and [1 1 0] steps. [1 0 0] steps are aligned along the closed-packed orientation and have strong nearest-neighbor interaction bondings along them, which makes them relatively smooth in equilibrium. In contrast to that, [1 1 0] steps are aligned along the direction geometrically farthest from the closed-packed orientation and, since we do not take second-nearest-neighbor interactions into account, have no bonding along them making them rough in equilibrium. Out of equilibrium, their behavior is also different. By modeling different mass transport mechanisms, we conclude that diffusion of step adatoms along the edge of the step provides a stabilization of step against roughening. We use a combination of our models for [1 0 0] and [1 1 0] to approximate steps of arbitrary orientation. For a specially constructed planar steady-state solution, we compute angular dependency of the step velocity and use it to construct a kinetic Wulff shape. Within such an approach, the growth velocities are likely to be underestimated, yet this does not affect the final kinetic Wulff shape.

Acknowledgement

This work was supported by DFG within SFB 611 Singular phenomena and scaling in mathematical model and SPP 1095 analysis, modeling and simulation of multiscale problems.

References

[1] T. Michely, J. Krug, Island Mounds and Atoms, Springer, 2004.
[2] A. Voigt (Ed.), Multiscale Modeling in Epitaxial Growth, Birkhäuser, 2005.
[3] W.K. Burton, N. Cabrera, F.C. Frank, Philos. Trans. R. Soc. London, Ser. A 243 (866) (1951) 299.
[4] L. Balykov, M. Kitamura, I. Maksimov, K. Nishioka, Philos. Mag. Lett. 78 (1998) 411.
[5] R.E. Caflisch, W.E.M.F. Gyure, B. Merriman, C. Ratsch, Phys. Rev. E 59 (6) (1998) 6879.
[6] R. Ghez, S.S. Iyer, IBM J. Res. Dev. 32 (1988) 804.
[7] G.S. Bales, A. Zangwill, Phys. Rev. B 41 (1990) 5500.
[8] L. Balykov, A. Voigt, Phys. Rev. E 72 (2) (2005) 022601.
[9] L. Balykov, A. Voigt, Multi. Model. Sim. 5 (2006) 45.
[10] J. Kallunki, J. Krug, Surf. Sci. 523 (2003) L53.
[11] J. Villain, A. Pimpinelli, Physique de la Croissance Cristalline, Editiones Eyrolles, 1995.
[12] G. Ehrlich, F.G. Hudda, J. Chem. Phys. 44 (1966) 1036.
[13] R.L. Schwoebel, E.J. Shipsey, J. Appl. Phys. 37 (1966) 3682.
[14] I.L. Aleiner, R.A. Suris, Sov. Phys. Solid. State 34 (1992) 809.
[15] Z. Zhang, M.G. Lagally, Science 276 (1997) 377.
[16] O. Pierre-Louis, M.R. D'Orsogna, T.L. Einstein, Phys. Rev. Lett. 82 (1999) 3661.
[17] T. Maroutian, L. Douillard, H.-J. Ernst, Phys. Rev. B 64 (2001) 165401.
[18] F. Nita, A. Pimpinelli, Phys. Rev. Lett. 95 (2005) 106104.
[19] M. Byckling, H. Junes, T. Jäevi, S. Pursiainen, A. Voigt, in: T. Eirola, V. Havu, A.-P. Jauho, J. von Pfaler (Eds.), Computational Problems in Physics 2005, vol. C018, Helsinki University of Technology, 2005, p. 31.
[20] L. Balykov, M. Kitamura, I. Maksimov, Europhys. Lett. 52 (2000) 692.
[21] D. Margetis, R.E. Caflisch, in preparation.
[22] T.J. Stasevich, T.L. Einstein, R.K.P. Zia, M. Giesen, H. Ibach, F. Szalma, Phys. Rev. B 70 (2004) 245404.
[23] R.F. Sekerka, Crys. Res. Technol. 40 (2005) 291.
[24] G. Wulff, Z. Krist. Mineral. 34 (1901) 449.
[25] J.E. Taylor, J. Cahn, C.A. Handwerker, Acta Mater. 40 (1992) 1443.